JOURNAL OF SOLID STATE CHEMISTRY **123,** 223–235 (1996)
ARTICLE NO. 0172

$La_{1-x}Sr_xCuO_{2.5}$ as a Doped Spin-Ladder Compound

Z. Hiroi

Institute for Chemical Research, Kyoto University, Uji, Kyoto-fu 611, Japan

Received October 6, 1995; in revised form February 2, 1996; accepted February 8, 1996

The high-pressure synthesis, structural characterization, and physical properties of $La_{1-x}Sr_xCuO_{2.5}$ ($0 \le x \le 0.20$) are reported. The nondoped $LaCuO_{2.5}$ prepared at high pressure of 6 GPa crystallizes in the $CaMnO_{2.5}$ structure which is one of the prototypes of anion-deficient perovskites. The Rietveld analysis of the powder X-ray diffraction pattern remarkably shows a quasi-one-dimensional structure composed of Cu–O ladders. The magnetic susceptibility measurements suggest a spin liquid ground state with a large energy gap of 490 K as theoretically expected for a $S = 1/2$ Heisenberg antiferromagnetic ladder system. Systematic hole-doping is achieved by substituting Sr for La. A dramatic insulator-to-metal transition has been observed in the resistivity measurements on doping, but, with no signs of superconductivity as predicted theoretically for a lightly doped spin-ladder system.

INTRODUCTION

Spin ladders have recently been of interest both theoretically and experimentally as low-dimensional quantum magnets (1, 2). They provide intermediate lattices existing between the one-dimensional (1D) $S = 1/2$ antiferromagnetic (AF) Heisenberg chain and the two-dimensional (2D) square lattice. In the former, quantum fluctuations prevent true long-range AF order, while the latter shows simple long-range order at low temperature. Ladder lattices of increasing width can be obtained by assembling chains one next to the other. Surprisingly, this crossover between one and two dimensions is not at all smooth (1–5). Ladders made of an even number of chains show a quantum spin liquid state or a short-range resonating valence bond state in which neighboring atoms are coupled to a spin singlet because of their purely short-range spin correlation. As a result, a finite energy gap, a so-called spin gap, exists in the spin excitation spectrum. In contrast ladders made of an odd number of chains display properties similar to a single chain, namely, gapless spin excitations.

This dramatic difference between even- and odd-chain ladders predicted by theory has now been confirmed experimentally in a series of cuprates $Sr_{n-1}Cu_nO_{2n-1}$ with $n = 2$ and 3 (6, 7). These compounds have been prepared at high pressure of 3–8 GPa (8, 9). They contain 2D Cu–O sheets which can be obtained by cutting the CuO_2 sheet into strips containing n Cu atoms in its width and then connecting them again so that the CuO_4 squares share edges at the interface. Because shearing resulted at the interface reduces effectively magnetic coupling between adjacent ladders, they are considered as quasi-1D magnetic systems. Moreover, the Cu^{2+} ion has one electron missing from a $3d$ shell, leaving the ion with a spin 1/2 magnetic moment, and these moments in each ladder are coupled antiferromagnetically through a strong AF superexchange interaction J via oxygen ions. Therefore, the ladder-type Cu–O lattice in these compounds can be considered as an actual representation of the theoretical spin-ladder model. In good agreement with theory, $SrCu_2O_3$ comprising two-chain ladders shows a well-defined spin gap with a magnitude of 400 K (6, 7), while $Sr_2Cu_3O_5$ comprising three-chain ladders shows true long-range order below 50 K (10).

A further intriguing theoretical prediction is the occurrence of superconductivity with a novel mechanism when even-chain ladders, namely, spin-liquid ground states, are lightly doped with holes (3, 4, 11–14). The physical picture based on a theoretical model called the t–J model (15) is rather straightforward in the case of isotropic two-chain ladders (Fig. 1): The ground state before doping consists of a set of spin singlets on each rung of the ladder, and the excitation can occur only at the expense of a definite energy to create a triplet on one of the rungs. The magnitude of the spin gap is calculated to be $J/2$. When lightly doped with holes, superconducting pairing correlations can be expected, because it is energetically more favorable to create hole pairs rather than to create free spins on different rungs. However, real materials appropriate to test this intriguing theoretical prediction have been limited only to the above mentioned cupric oxide and another two-chain ladder compound, $(VO)_2P_2O_7$ (16, 17), and it has been impossible to dope these with carriers. To be reported here is the preparation at high pressure and characterization of a new two-chain ladder compound, $LaCuO_{2.5}$, which can be rendered metallic by doping with holes (18).

0022-4596/96 $18.00

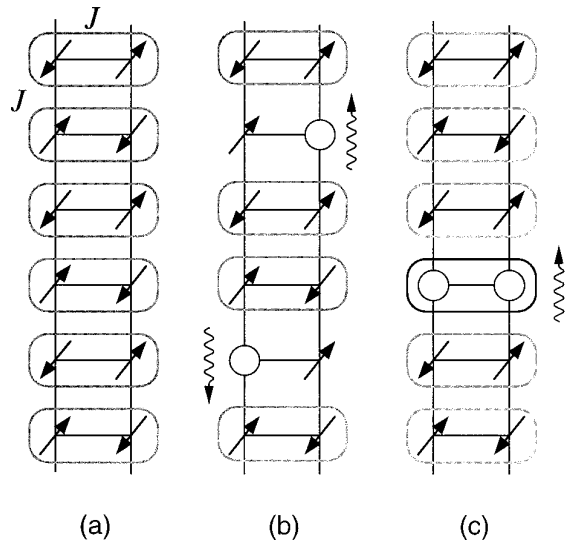

FIG. 1. Simplified representation of the two-chain spin ladder model proposing a possible occurrence of superconductivity (40). The arrows and circles represent 1/2 spins and doped holes, respectively. A nondoped ladder consists of a set of spin singlets (a). Doping with one hole breaks three AF bonds, giving rise to an energy loss proportional to 3*J*. When two holes are introduced and move independently of each other, the total energy loss is 6*J* (b). However, if they occupy sites on opposite sides of a rung, it becomes only 5*J*. This energy gain could lead to pairing correlations, and, thus, 1D superconductivity of the purely electronic origin could occur on lightly doped spin ladders. See Refs. (1–5) for elaborate discussion.

There are three known compounds, La_2CuO_4, $La_8Cu_7O_{19}$, and $La_2Cu_2O_5$, in the La_2O_3–CuO system at normal synthetic conditions. The first one is the parent material of the first high-T_c cupric oxide superconductor, $La_{2-x}Ba_xCuO_4$ (19), and the others are members of homologous series with the general formula $La_{4+4n}Cu_{8+2n}O_{14+8n}$ (20). The structure of the homologous series is rather complicated, based on the insertion of La_2CuO_4-type ribbons of different widths between CuO planes of a complex geometry. Besides these compounds, $LaCuO_{3-\delta}$ has been prepared under high oxygen pressures which crystallizes in a distorted perovskite structure (21, 22), and $LaCuO_2$ under reducing atmosphere (23). I have explored a new compound in this pseudo-binary system under high pressure of 6 GPa and found that $La_2Cu_2O_5$ undergoes structural transformation at high pressure into a simple oxygen-deficient perovskite structure ($CaMnO_{2.5}$ type). The high-pressure (HP) product is denser by 3% than the complex ambient pressure (AP) form. Hereafter, we will call the compound of the $CaMnO_{2.5}$ structure a $LaCuO_{2.5}$. In a previous study it was reported that $LaCuO_{2.5}$ of the $CaMnO_{2.5}$ structure was obtained at ambient pressure by low-temperature reduction of $LaCuO_{3-\delta}$ prepared at high oxygen pressure (24).

Since the Sr substitution for La is the most popular technique to dope lanthanum copper oxides with hole carriers, the ternary system La_2O_3–SrO–CuO has been extensively studied (25). On the perovskite line of (La, Sr)/Cu = 1/1 a few compounds crystallizing in various oxygen-deficient perovskite structures have been reported. $(La_{1-y}Sr_y)_8Cu_8O_{20-\delta}$ has a tetragonal cell of $a \approx 2\sqrt{2}a_p$, $c \approx a_p$ (a_p is the lattice parameter of the primitive cubic perovskite) for $0.16 \leq y \leq 0.24$ (25, 26), $\delta \approx 0$ and $0.7 \leq y \leq 0.8$, $\delta \approx 4$ (27), which involves three types of copper coordination, octahedral, pyramidal, and square planar. Interestingly, Otzschi *et al.* carefully studied on this phase line and found a $CaMnO_{2.5}$-type perovskite only for a narrow composition range around $y = 0.14$ as a low-temperature form of the above perovskite (28).

Application of high pressure is known to change phase stability dramatically in various systems. In the case of complex copper oxides it has been clearly demonstrated by showing that the unusual oxygen-deficient "perovskite" structure of a $CuO_2/A/CuO_2$ sequence, which is called an infinite-layer structure (29), is stabilized for *A* cations of wide alkaline-earth metal compositions in $ACuO_2$ (30). It is also the case for the present system. A systematic Sr substitution for La up to 20% in $LaCuO_{2.5}$ has been made possible under high pressure.

Here we report the high-pressure synthesis of $LaCuO_{2.5}$ and $La_{1-x}Sr_xCuO_{2.5}$. The structural characterizations indicate that these compounds are to be considered as having a quasi-one-dimensional lattice made of Cu–O ladders rather than a three-dimensional perovskite network. The magnetic properties are also reported, suggesting the formation of a pseudo-spin gap for the nondoped compound as expected from its crystal structure. The electrical resistivity measurements show a marked insulator-to-metal transition as a function of Sr content.

EXPERIMENTAL

High-pressure synthesis. A base material of $La_2Cu_2O_5$ was prepared following the method reported by Cava *et al.* (20), starting from La_2O_3 (dried at 1000°C in air) and CuO in appropriate molar proportions. In order to avoid a contamination with La_2CuO_4 special cares were taken to keep the furnace temperature at 1000°C while inserting or removing the pellets, because the material is stable only in the narrow temperature range 999–1012°C (20): La_2CuO_4 is also stable at high pressure and would remain as an impurity after high-pressure heat treatments. The oxygen content of the single-phase material was determined by heating to 800°C in 95% N_2–5% H_2 and measuring the weight loss. This yielded the approximate stoichiometry of $La_2Cu_2O_5$ as reported previously (20).

To replace La by Sr, other base materials, $(La_{1-y}Sr_y)_8Cu_8O_{20}$ with $y = 0.20$, 0.25, 0.30, were prepared from La_2O_3, $SrCO_3$, and CuO by firing at 980°C in air. They

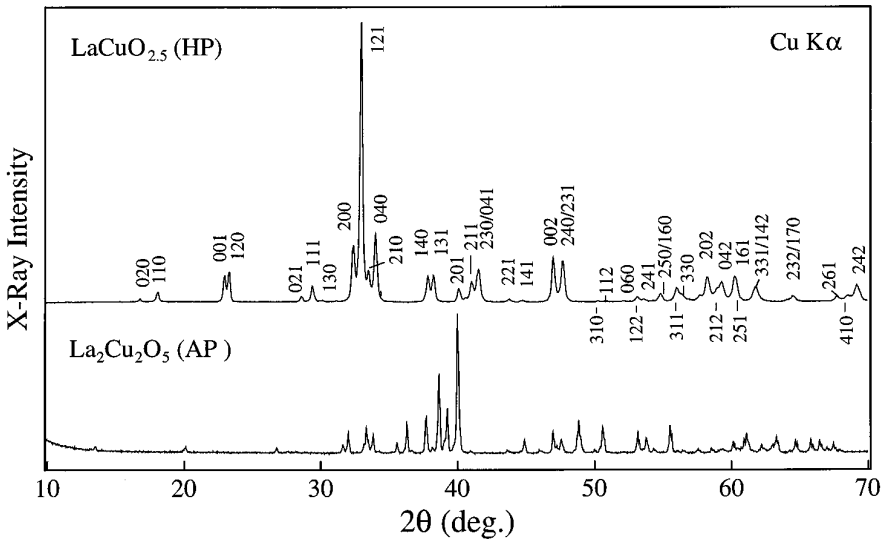

FIG. 2. Powder X-ray diffraction patterns of the starting material $La_2Cu_2O_5$ prepared at ambient pressure and the high-pressure product $LaCuO_{2.5}$. All the visible peaks in the latter are indexed with an orthorhombic cell of edges $a = \sqrt{2}a_p$, $b = 2\sqrt{2}a_p$, $c = a_p$. No contaminations with La_2CuO_4, CuO, and the starting material are seen.

were monophasic for $y = 0.2$ and 0.25 as examined by the X-ray diffraction method, crystallizing in a tetragonal structure of $a \approx 2\sqrt{2}a_p$ and $c \approx a_p$ as reported previously (26). The oxygen content determined by the hydrogen reduction method gave 20 within the experimental precision of ± 0.1, indicating an approximate copper valence of $2 + y$. The product for $y = 0.30$ contained CuO as an impurity phase.

Powders of $La_2Cu_2O_5$ or appropriate mixtures of $La_2Cu_2O_5$ and $(La_{1-y}Sr_y)_8Cu_8O_{20}$ ($y = 0.2$ for $0 < x \leq 0.2$; $y = 0.25$ for $0.2 < x \leq 0.25$; $y = 0.30$ for $0.25 < x \leq 0.30$) were sealed in gold capsules, pressed almost isostatically up to 6 GPa using a cubic-anvil-type HP apparatus (31), and heat treated at 800–900°C for 30 min. Then, temperature was dropped to room temperature within a few seconds before releasing the pressure. A typical weight of the products was 250 mg. They were all stiff and black in color, and quite stable in air at room temperature and ambient pressure.

Characterization. The HP products were characterized by means of powder X-ray diffraction (XRD), electron diffraction (ED), and high-resolution electron microscopy (HREM). The XRD measurements were performed on a Rigaku rotating anode diffractometer with graphite monochromatized Cu$K\alpha$ radiation. Data for the Rietveld analysis were collected at room temperature over the 2θ range 16°–120° at a 0.03° step for 10 sec which included 291 reflections. Structural refinements were performed using the Rietveld software Rietan working on a Macintosh computer (32). Low temperature XRD measurements were also done at temperatures between 10 and 300 K. Si powders were mixed with sample powders as an internal standard. The temperature dependence of the lattice parameters were determined using the Rietveld refinement technique, assuming that of Si was constant ($a = 5.4315$ Å) against temperature change, because its overall temperature dependence ($\sim 5 \times 10^{-4}$ Å) was almost within the estimated standard deviations of the refinements.

ED and HREM experiments were carried out on a JEOL-2000EX electron microscope equipped with a top-entry goniometer stage operating at 200 kV. Specimen for observations were prepared by crushing pellets in acetone and collecting fragments on carbon-coated holey film supported by a copper grid. Simulations for HREM images were done using the MacTempus software.

Electrical resistivity was measured by a standard four-probe method between 5 and 300 K. Magnetic susceptibility was measured on a Quantum Design SQUID magnetometer in an applied magnetic field of 1 T typically from 5 to 350 K and sometimes between 2 and 550 K with raising temperature after cooling in a nearly zero magnetic field. Absence of hysteresis behavior between heating and cooling under the magnetic field was seen for several non-doped and doped samples.

RESULTS AND DISCUSSION

$LaCuO_{2.5}$

Structural characterization. The XRD profile for the present lanthanum copper oxide has completely changed after the HP treatment as shown in Fig. 2, implying that a structural transformation has occurred at certain pressure

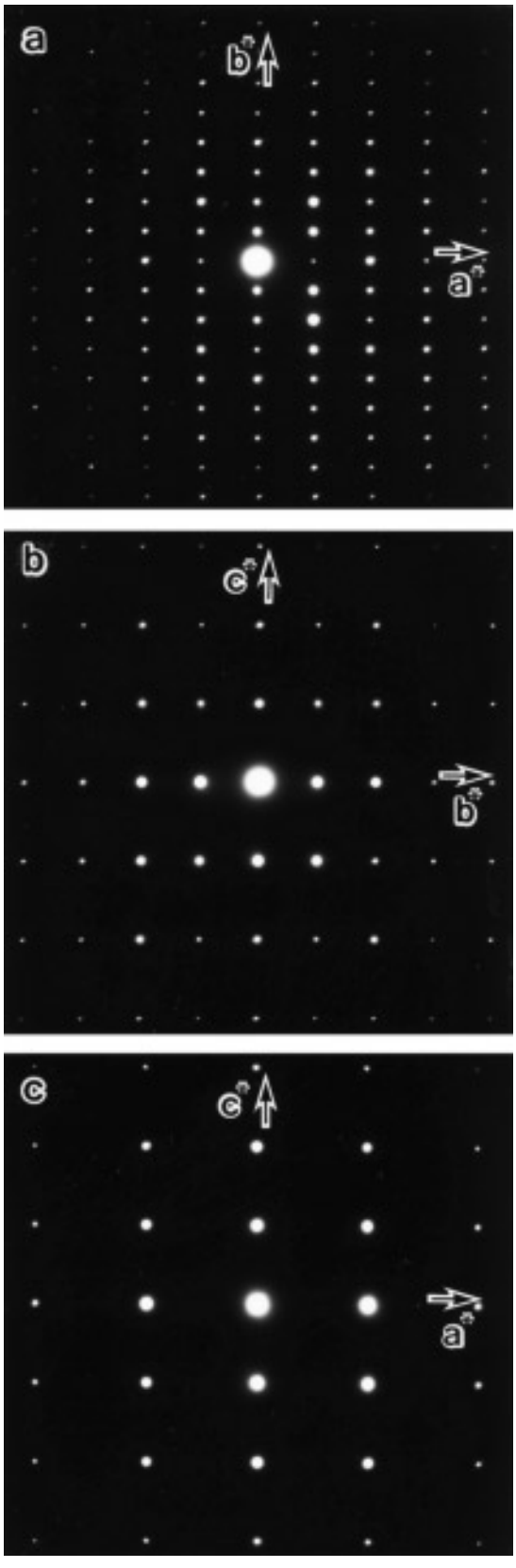

below 6 GPa. The pattern for the HP product shows the most intense peak at $2\theta \sim 33$ ($d \sim 2.7$ Å) and a couple of peaks at $2\theta \sim 23°$ ($d \sim 3.9$ Å), which suggests the product to be of perovskite type. The ED experiments clearly supported this, revealing an orthorhombic unit cell of $\sqrt{2}a_p \times 2\sqrt{2}a_p \times a_p$. Figure 3 shows three representative zone axis ED patterns. The rectangular mesh in the [001] zone (a) corresponds to a $\sqrt{2}a_p \times 2\sqrt{2}a_p$ unit in real space. Extinctions are seen in the [100] and [010] zone axis patterns; ($0kl$) for $k = 2n$, ($0k0$) for $k = 2n$, ($h0l$) for $h = 2n$, and ($h00$) for $h = 2n$. The ($h00$) and ($0k0$) reflections with h, $k = 2n + 1$ in the [001] pattern are due to double diffraction. The possible space group deduced from the extinctions is *Pbam* or *Pba*2. Based on the unit cell and the space group, all the visible peaks in the XRD pattern could be indexed consistently as shown in Fig. 2. No contaminations with La_2CuO_4, CuO, and AP $La_2Cu_2O_5$ were detected, which means that the structural transformation is polymorphic. The oxygen content of the HP phase was 2.48 ± 0.02 as determined by the hydrogen reduction method.

These results indicate the $CaMnO_{2.5}$ structure (space group *Pbam*) which is one of the prototypes of anion-deficient perovskites (33). It is quite natural that a generally dense perovskite structure is stabilized under high pressure and also that this copper oxide crystallizes in the $CaMnO_{2.5}$ structure instead of another typical prototype $CaFeO_{2.5}$ structure, because Cu^{2+} is a Jahn–Teller ion just as Mn^{3+}.

Rietveld refinement. The structural parameters have been refined using the Rietveld analysis technique. The atomic coordinates for $CaMnO_{2.5}$ were used as a starting point for the refinement (33). The occupancies of all the atoms were fixed to 1 and the isotropic thermal parameters for the oxygen atoms were fixed to 1 Å^2. The observed, calculated, and difference diffraction profiles are shown in Fig. 4. A good fitting was achieved with convergence to low agreement factors; $R_{wp} = 3.4\%$, $R_R = 7.5\%$, $R_e = 3.9\%$, and $S = 0.87$. A possible reason for the too small goodness-of-fit parameter S less than 1 is the high background of the data arising from copper fluorescence, which can also give rise to underestimation of the estimated standard deviations of fitting parameters. Final cell, positional, and isotropic thermal parameters are given in Table 1 in addition to selected bond distances. Details of the structure will be described later. Here we just compare these parameters with the previous results on $LaCuO_{2.5}$ prepared from $LaCuO_3$ (24). A few differences are noticed: For example, the lattice parameters a and c are nearly the same (within

FIG. 3. Electron diffraction patterns of $LaCuO_{2.5}$ along the three main zone axes; (a) [001], (b) [100], and (c) [010]. The ($h00$) and ($0k0$) reflections with h, $k = 2n + 1$ appear in the [001] zone owing to double diffraction.

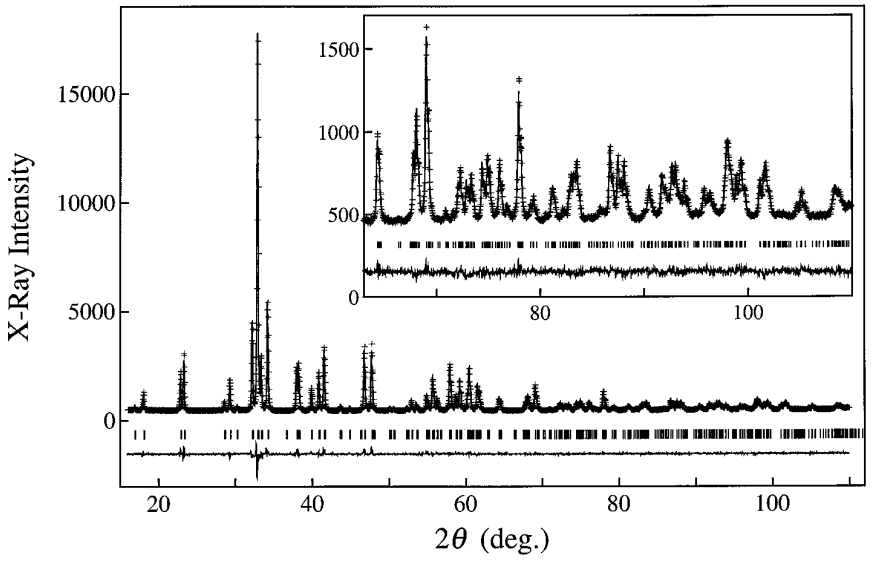

FIG. 4. Rietveld refinement profiles for $LaCuO_{2.5}$. The crosses represent the observed data, and the solid line is a calculated profile. A difference plot is also shown below them. The refined structural parameters are summarized in Table 1.

10^{-3} Å) between the two compounds, while the *b* axis is considerably shorter by ~0.01 Å for the HP product. This suggests that the two $LaCuO_{2.5}$ have slightly different structures, arising from different synthetic routes.

High-resolution electron microscopy. Microstructures of $LaCuO_{2.5}$ prepared at high pressure have been investigated by means of HREM. The crystals examined were almost defect-free, and no other types of superstructure possibly arising from different ways of oxygen vacancy ordering were seen. Figure 5 reproduced a typical HREM image taken with the incident electron beam parallel to the *c* axis together with a series of images calculated based on the refined structural parameters as a function of crystal thickness. A fairly good agreement between them is noted: Though oxygen vacancies are generally difficult to be directly imaged in HREM, an array of paired bright dots, which must reflect the characteristic deviation from the ideal cubic perovskite, is pronounced in the thicker part of crystals in both the experimental and calculated images.

TABLE 1
Refined Structural Parameters of $LaCuO_{2.5}$

Atom	Position	*x*	*y*	*z*	B_{iso} (Å^2)
La	4*h*	0.3122(1)	0.3602(1)	0.5	0.28(2)
Cu	4*h*	0.2928(3)	0.1057(2)	0	0.38(4)
O(1)	4*g*	0.2824(10)	0.1071(7)	0.5	1.0
O(2)	4*g*	0.0882(12)	0.2951(6)	0	1.0
O(3)	2*a*	0	0	0	1.0

Selected bond distances (Å)

Cu–O(2)	1.941(5)	[1×]	La–O(2)	2.403(3)	[2×]
Cu–O(1)	1.941(1)	[2×]	La–O(1)	2.631(5)	[1×]
Cu–O(3)	1.965(2)	[1×]	La–O(1)	2.638(6)	[1×]
Cu–O(2)′	2.285(5)	[1×]	La–O(3)	2.644(1)	[2×]
			La–O(1)	2.654(6)	[1×]
			La–O(2)	2.958(4)	[2×]
			La–O(1)	2.959(5)	[1×]

Note. Space group *Pbam* (No. 55); $a = 5.5482(1)$ Å, $b = 10.4677(1)$ Å, $c = 3.8801(1)$ Å; $Z = 4$ formula unit per unit cell; $R_{wp} = 3.4\%$, $R_p = 2.3\%$, $R_R = 7.5\%$, $R_e = 3.9\%$, $S = 0.87$. Estimated standard deviations in parentheses refer to the last digit. Isotropic thermal parameters, B_{iso}, were refined for sites La and Cu and fixed for the oxygen sites.

Description of the structure. In the ideal $CaMnO_{2.5}$ structure one fourths of oxygen atoms are missing from MnO_2 sheets so as to form an ordered array of one-dimensional channels of vacancies which run along the *c* axis (Fig. 6a). The Mn–O sublattice consists of corner-shared MnO_5 square pyramids. On the other hand, the apical oxygens of the MnO_5 square pyramids shift away slightly in real $CaMnO_{2.5}$ because of a Jahn–Teller distortion (33). A similar distortion occurs in $LaCuO_{2.5}$. However, the elongation of the transition metal–O(apex) bonds is much larger (2.29 Å) in the latter than in the former (2.09 Å). Moreover, the positions of transition metals shift much more from the ideal positions in the copper oxide, which results in remarkable pairing of Cu atoms within the basal plane (Fig. 6b). Therefore, as a structural component appropriate to describe $LaCuO_{2.5}$ we should not take a square pyramid as in $CaMnO_{2.5}$ but a ladder which consists of a couple of corner-shared CuO_4 planar squares linked by corners along the *c* axis as perspectively illustrated in Fig. 7. Note that Cu and O atoms are almost coplanar in each ladder. As a result, the structure of $LaCuO_{2.5}$ is very exceptional among many perovskite based structures in the sense

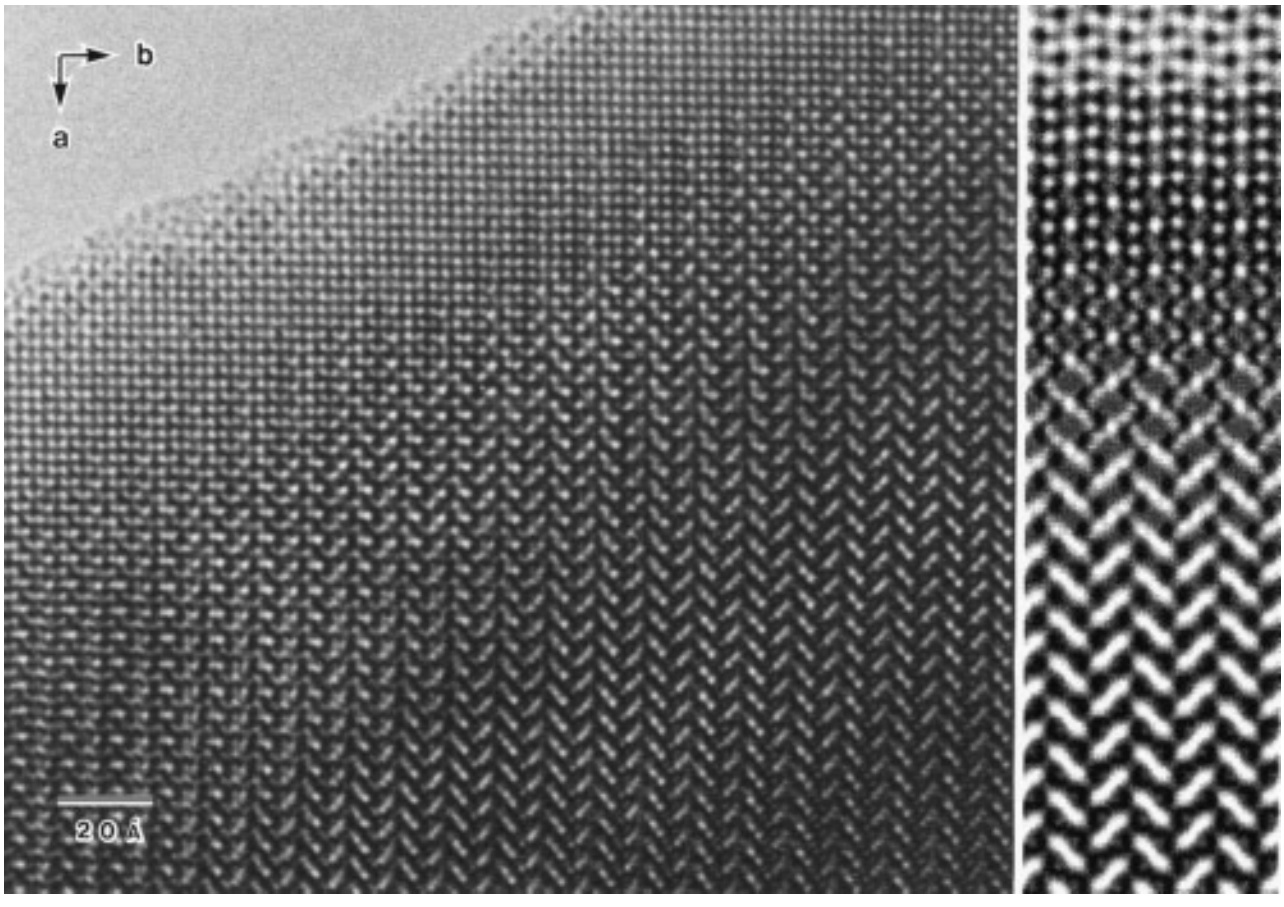

FIG. 5. High-resolution electron microscopy image taken with the incident electron beam parallel to [001] at 200 kV (left) and a series of computer-simulated images as a function of crystal thickness between 8 and 80 Å in a 8 Å step with each image having a $2a \times 3b$ unit cell (right). The electron-optical parameters used are $E = 200$ kV, $C_s = 1.2$ mm, $\Delta = 100$ Å, $\alpha = 0.5$ mrad, and $\Delta f = -650$ Å.

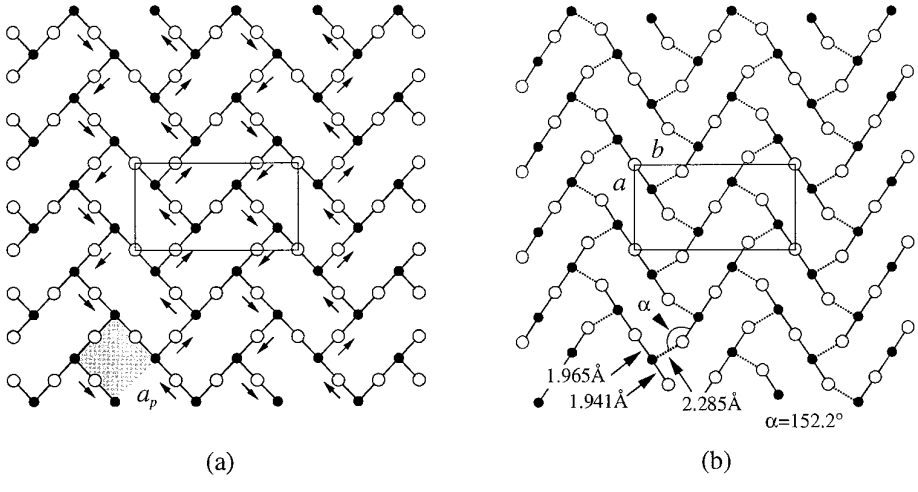

FIG. 6. Schematic structures of the transition-metal oxygen plane for the ideal $CaMnO_{2.5}$ structure (a) and $LaCuO_{2.5}$ (b). The small filled and the large open circles show the positions of transition metals and oxygens, respectively. A projected unit cell of $\sqrt{2}a_p \times 2\sqrt{2}a_p$ is drawn by a rectangle in each figure. Metal–oxygen bonds shorter (longer) than 2 Å are shown with solid (broken) lines. The arrows in (a) indicate the directions of oxygen movement due to a Jahn–Teller distortion.

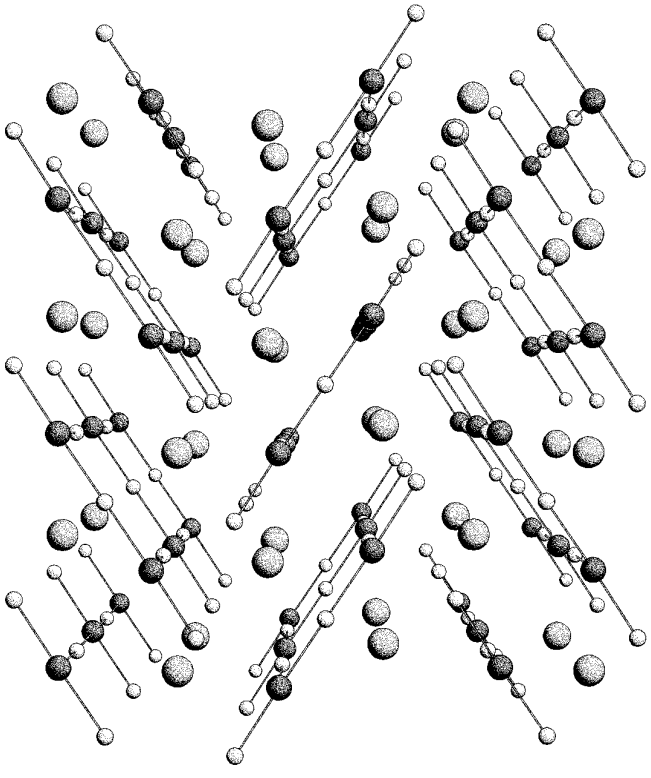

FIG. 7. Perspective view of $LaCuO_{2.5}$ along the c axis. Large, medium, and small balls represent La, Cu, and O atoms, respectively.

that it is quasi-one-dimensional rather than three-dimensional.

Furthermore, one-dimensional character in physical properties would be expected from this unique structure, if one considers anisotropy of the magnitudes of electron transfers and antiferromagnetic interactions between neighboring Cu atoms via oxygen atoms. Strong antiferromagnetic interactions should occur within each ladder, because the Cu–O–Cu bond length is short and the angle is nearly 180°. In contrast, the long Cu–O(apex) bond length and the nonlinear Cu–O(apex)–Cu bond angle (152°) lead us to assume that antiferromagnetic interactions are much weaker between two Cu atoms in adjacent ladders. More importantly, this unbalanced Cu–O configuration must make unpaired electrons confined in the intra-ladder Cu d_{x2-y2}–O $2p_\sigma$ orbitals (see Fig. 13). Thus, inter-ladder interactions will be further weakened as a result of the approximate orthogonality (68.5°) between adjacent ladders, because electron transfer between mutually orthogonal orbitals is prohibited by symmetry. These considerations lead us to assume that each ladder is considerably isolated from the others and provides a quasi-one-dimensional electronic system. However, recent band structure calculations have suggested that half-filled σ^* bands near the Fermi level exhibit anisotropic rather than 1D characteristics because of considerably large contribution from Cu d_{z^2} orbitals. It seems more realistic to consider $LaCuO_{2.5}$ as a strongly coupled ladder system in comparison with $SrCu_2O_3$.

Low-temperature XRD. Structures at low temperatures have been investigated by powder XRD measurements as a function of temperature between 10 and 300 K. The overall diffraction profile at 10 K remained essentially the same as that at 300 K: Neither peak splitting nor selective broadening were detected. The Rietveld analysis confirmed that the structure was essentially the same. The temperature dependence of the lattice parameters is plotted in Fig. 8. The lattice shrinks almost isotropically by 0.15% down to 10 K.

Physical properties. Since the valence state for Cu is +2 for both AP $La_2Cu_2O_5$ and HP $LaCuO_{2.5}$, they are almost insulating because of large electron correlation. The

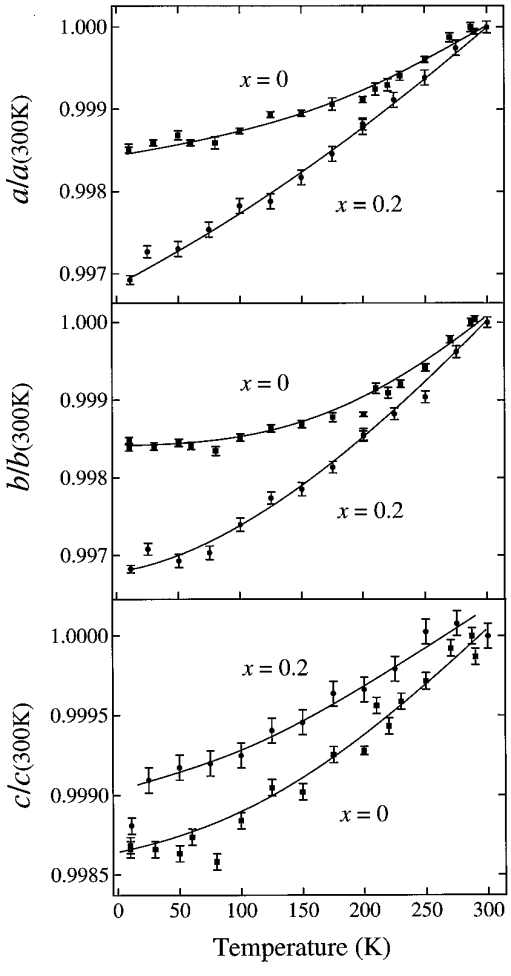

FIG. 8. Temperature dependence of the lattice parameters normalized at 300 K for $La_{1-x}Sr_xCuO_{2.5}$ determined by powder XRD measurements. The error bars show the estimated standard deviations deduced from the Rietveld refinements. The solid lines are guides to the eye.

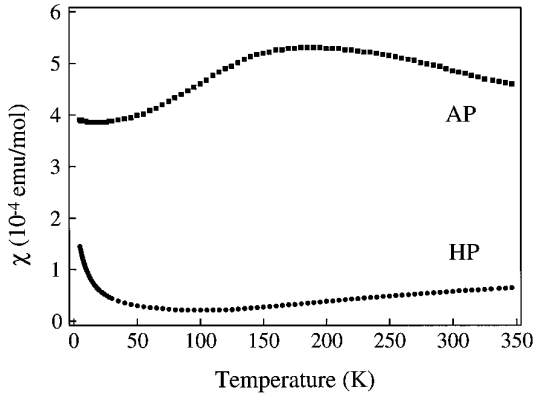

FIG. 9. Comparison of the magnetic susceptibility χ between the AP and HP phases.

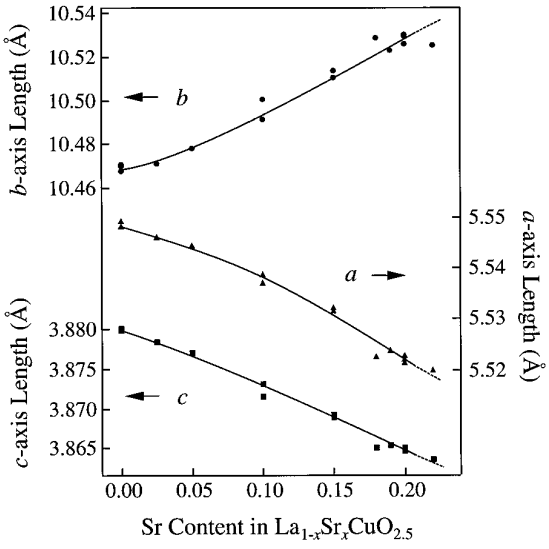

FIG. 11. Variation of the lattice parameters as a function of Sr content in $La_{1-x}Sr_xCuO_{2.5}$. The samples are monophasic for $x \leq 0.20$, but contain a small amount of $(La_{1-y}Sr_y)_8Cu_8O_{20}$ for $x = 0.22$. The estimated standard deviation of each datum deduced from the Rietveld analysis, which is not shown, is small almost within the mark. The solid lines are guides to the eye.

electrical resistivity of $LaCuO_{2.5}$ will be reported later. Magnetic susceptibility has obviously changed after the HP treatment as compared in Fig. 9. The magnitude is reduced by an order, and the broad peak near 190 K for the AP phase seems to shift to much higher temperature for the HP phase. These suggest that antiferromagnetic magnetic interactions are much stronger in the HP phase.

Most important here is to address whether the Cu–O ladders suggested from the above structural considerations really behave as spin ladders consisting of antiferromagnetically coupled $S = 1/2$ antiferromagnetic chains. Looking in detail at the temperature dependence of the magnetic susceptibility between 4.5 and 550 K which is shown in Fig. 10, we see that it decreases gradually with decreasing temperature to a minimum near 100 K with a convex curvature. A continuous Curie-like increase is seen at lower temperature. The minimum value at 100 K is reduced less than one forth of the value at 550 K. The data cannot be fitted to the Borner–Fisher-type magnetic susceptibility for low-dimensional antiferromagnets because the observed decrease is much larger than expected. Thus, we have assumed a nonmagnetic ground state with a spin-excitation

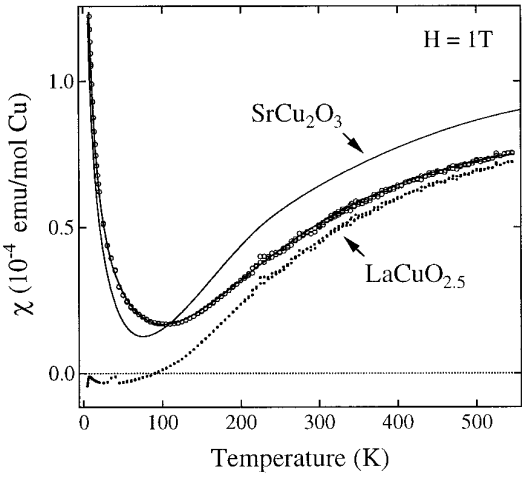

FIG. 10. Temperature dependence of the magnetic susceptibility of $LaCuO_{2.5}$. The data (open circles) were collected in two runs: The first run was carried out, after zero-field cooling, with increasing temperature and then decreasing between 4.5 and 350 K at an applied magnetic field of 1 T. The second run was done similarly between 300 and 550 K. No significant hysteresis behaviors are seen. The solid line on the data points shows the result of fitting to the equation in the text, and the dotted line represents the susceptibility after reduction of the Curie component. The raw data of $SrCu_2O_3$ are shown for comparison.

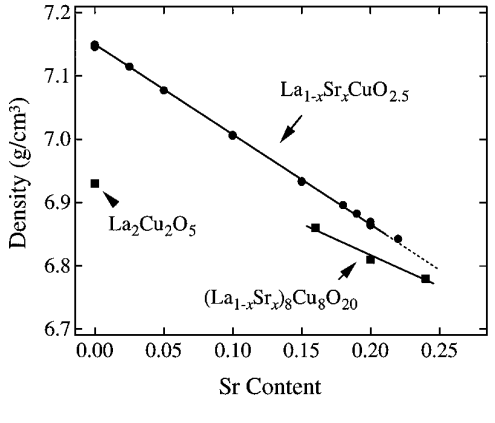

FIG. 12. Calculated density of $La_{1-x}Sr_xCuO_{2.5}$, $La_2Cu_2O_5$ (20), and $(La_{1-y}Sr_y)_8Cu_8O_{20}$ (26, 41) versus Sr content.

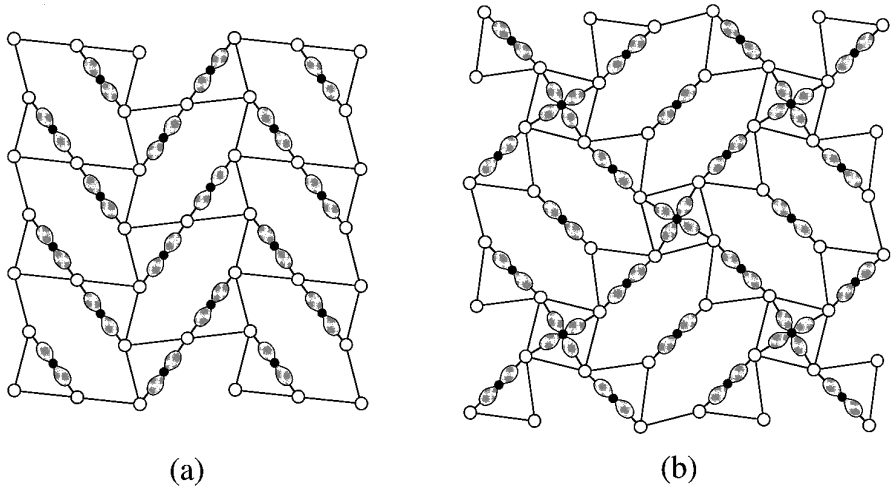

FIG. 13. Schematic drawings of the Cu–O plane for HP $La_{0.8}Sr_{0.2}CuO_{2.5}$ (a) and AP $(La_{0.8}Sr_{0.2})_8Cu_8O_{20}$ (b). The atomic positions are exactly shown, based on the Rietveld refinement in each case. Only the Cu d_{x2-y2} orbitals lying on the plane are shown.

gap due to singlet correlations in spin ladders, and fitted the data to the equation

$$\chi = \chi_0 + C/(T - \Theta) + \alpha T^{-1/2} \exp(-\Delta/T),$$

where χ_0 is a temperature independent term, and the second term is a Curie–Weiss contribution ascribed to impurities and/or Cu^{2+} ions made free by crystal imperfections. The third term represents the bulk spin susceptibility expected for a two-chain spin 1/2 Heisenberg AF ladder, where α is a constant factor and Δ is the magnitude of the spin gap (34). The result of fitting was very good as shown by the solid line on the data points in Fig. 10. The obtained values are $\chi_0 = -2.2(2) \times 10^{-6}$ emu/mol, $C = 1.66(1) \times 10^{-3}$ emu/mol, $\Theta = -5.45(8)$ K, $\alpha = 4.26(1) \times 10^{-3}$, and $\Delta = 492(2)$ K. All these values are very similar to those reported for $SrCu_2O_3$(6). Since χ_0 is close to the sum of the temperature-independent contributions of the core diamagnetism (-6.2×10^{-5} emu/mol) and the Van Vleck paramagnetism (6.0×10^{-5} emu/mol) (35), the spin excitation is likely suppressed at low temperature. The amount of free Cu^{2+} spins calculated from the Curie component is only 0.38%.

For an isolated two-chain spin ladder the spin gap has been calculated to be $J/2$, where J is the intra-ladder antiferromagnetic exchange. Although an accurate value of J is not known, this should be about 1300 K on the analogy of the usual CuO_2 plane with the linear Cu–O–Cu configuration. However, it has been also theoretically pointed out that an inter-ladder antiferromagnetic exchange coupling J' would strongly suppress the magnitude of spin gap (4). In the case of $SrCu_2O_3$, $J'/J = 0.1$ has been estimated. The fact that the magnitude of the spin gap for $LaCuO_{2.5}$ is comparable to that for $SrCu_2O_3$ (400 K) suggests that inter-ladder interactions are still weak in $LaCuO_{2.5}$ as in $SrCu_2O_3$.

The above-mentioned magnetic susceptibility measurements are consistent with a spin-liquid picture for $LaCuO_{2.5}$. However, it is still controversial, because recent NMR experiments on $LaCuO_{2.5}$ have suggested that an unusual magnetic order with tiny moments takes place below 120 K as evidenced by a large enhancement of the nuclear spin-lattice relaxation rate ($1/T_2$) instead of an exponential decrease and the disappearance of the Cu-NMR signal (36). Moreover, very recent μSR experiments also pointed out the existence of magnetic order below 120 K (37). It would be unusual if a true 3D AF order develops below such a high temperature in spite of the observed large reduction in spin susceptibility. However, it may be reasonable to assume that the ground state of $LaCuO_{2.5}$ lies between a singlet spin-liquid state and a Neel ordered state because of rather strong inter-ladder coupling. Then, a singlet correlation would be dominant at high temperature, while a crossover into a long-range ordered state could be expected with decreasing temperature. In this sense it is more reasonable to interpret the observed reduction in magnetic susceptibility as indicating the opening of a pseudo-gap arising from singlet correlation within the ladders.

$La_{1-x}Sr_xCuO_{2.5}$

Phase stability. The systematic replacement of La by Sr can be achieved under high pressure without any significant modifications of structure. This is in contrast to the previous results that only the composition near $x = 0.14$ is stabilized in the $CaMnO_{2.5}$ structure at ambient pressure and low temperature (28). A continuous variation in the

TABLE 2
Refined Structural Parameters of $La_{0.8}Sr_{0.2}CuO_{2.5}$

Atom	Position	x	y	z	B_{iso} (Å^2)
La/Sr[a]	4*h*	0.3081(3)	0.3605(2)	0.5	0.31(4)
Cu	4*h*	0.2874(7)	0.1069(4)	0	0.40(8)
O(1)	4*g*	0.2960(21)	0.0959(13)	0.5	1.0
O(2)	4*g*	0.0596(26)	0.2841(12)	0	1.0
O(3)	2*a*	0	0	0	1.0
Selected bond distances (Å)					
Cu–O(2)	1.891(13)	[1×]	La–O(2)	2.503(9)	[2×]
Cu–O(1)	1.937(1)	[2×]	La–O(1)	2.544(14)	[1×]
Cu–O(3)	1.945(5)	[1×]	La–O(3)	2.649(1)	[2×]
Cu–O(2)′	2.251(15)	[1×]	La–O(1)	2.733(12)	[1×]
			La–O(1)	2.788(14)	[1×]
			La–O(2)	2.825(9)	[2×]
			La–O(1)	2.865(12)	[1×]

Note. Space group *Pbam* (No. 55); $a = 5.5221(1)$ Å, $b = 10.5295(2)$ Å, $c = 3.8650(1)$ Å; $Z = 4$ formula unit per unit cell; $R_{wp} = 3.9\%$, $R_p = 2.8\%$, $R_R = 9.0\%$, $R_e = 3.5\%$, $S = 1.10$. Estimated standard deviations in parentheses refer to the last digit. Isotropic thermal parameters, B_{iso}, were refined for sites La/Sr and Cu and fixed for the oxygen sites.

[a] Refined occupancy of Sr is 0.184(7) under constraints, $g(La) + g(Sr) = 1$, $x(La) = x(Sr)$, $y(La) = y(Sr)$, $z(La) = z(Sr)$, $B_{iso}(La) = B_{iso}(Sr)$.

TABLE 3
Selected Distances and Angles for $La_{1-x}Sr_xCuO_{2.5}$

	$x = 0$	$x = 0.2$
Distances (Å)		
Cu–Cu (leg)	3.880(0)	3.865(0)
Cu–Cu (lung)	3.930(3)	3.891(9)
Cu–Cu (inter-ladder)	4.102(2)	4.088(6)
Cu–O(apex)	2.285(5)	2.251(15)
Angles (°)		
Cu–O(apex)–Cu	152.2(3)	161.4(7)
Cu–O(leg)–Cu	176.5(3)	172.6(8)
Cu–O(lung)–Cu	180	180
O(lung)–Cu–O(edge)	176.5(2)	178.0(5)
ladder–ladder	68.5	70.7

lattice parameters as a function of Sr content is shown in Fig. 11. The decrease of a and c indicates a shrinkage of the hole-doped Cu–O ladders, while the increase of b results from the rotation of each ladder which will be discussed later.

The samples of $x \leq 0.2$ were monophasic without $La_{2-x}Sr_xCuO_4$, CuO or the AP phases, whereas the sample of $x = 0.22$ contained a small amount of $(La_{1-y}Sr_y)_8Cu_8O_{20}$. Thus, the solubility limit must lie between $x = 0.20$ and 0.22 at 6 GPa. The AP structure remained intact for $x = 0.25$ and 0.30. It is interesting to note that the $(La_{1-y}Sr_y)_8Cu_8O_{20}$ phase is stable only for $0.15 \leq y \leq 0.24$ at ambient pressure (26), while the application of high pressure stabilizes it even for $x = 0.30$. The lattice parameters previously reported for $La_{0.857}Sr_{0.143}CuO_{2.5}$ of the $CaMnO_{2.5}$ structure are $a = 5.526$, $b = 10.503$, and $c = 3.865$ Å (28), which do not fall on the lines in Fig. 11, suggesting a slight difference in the way of oxygen ordering.

In order to discuss the phase stability under high pressure it is generally significant to compare the density of a HP phase with that of the corresponding AP phase. Figure 12 compares the calculated density as a function of Sr composition. The difference between the HP and AP phases is largest, ~3%, for the nondoped materials and becomes smaller around $x = 0.20$, where the HP phase disappears. This gives a reasonable explanation for the observed stability limit for the HP phase, because a gain in free energy ($\Delta G = P\,\Delta V$) at elevated pressure must determine the phase stability, which may be insufficient for $x > 0.20$ to induce the structural transformation. The density of $La_{0.857}Sr_{0.143}CuO_{2.5}$ prepared at low temperature is calculated to be 6.95 g/cm^3 (28), which approximately falls on the line for the high pressure phase in Fig. 12. This means that the dense form is also stabilized at low temperature and ambient pressure in the specific composition.

It is interesting to further compare $La_{1-x}Sr_xCuO_{2.5}$ and $(La_{1-y}Sr_y)_8Cu_8O_{20}$ with respect to the dimensionality of electronic structures. Figure 13 illustrates two corresponding structures of the Cu–O plane for $x = 0.20$, each of

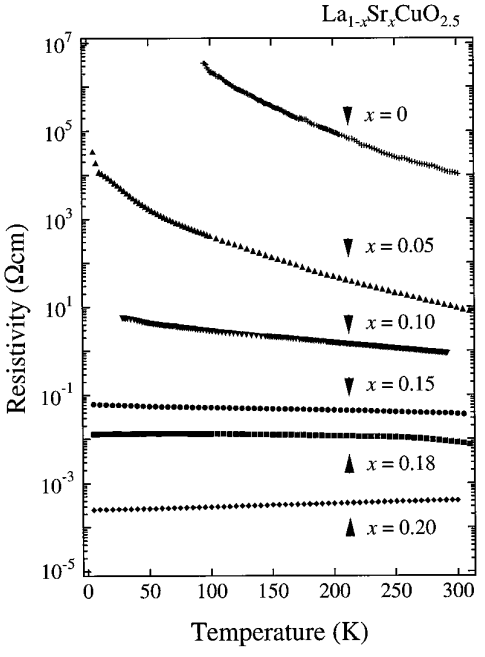

FIG. 14. A series of electrical resistivity versus temperature curves showing a systematic decrease of the amplitude upon doping and an insulator-to-metal transition at x between 0.18 and 0.20.

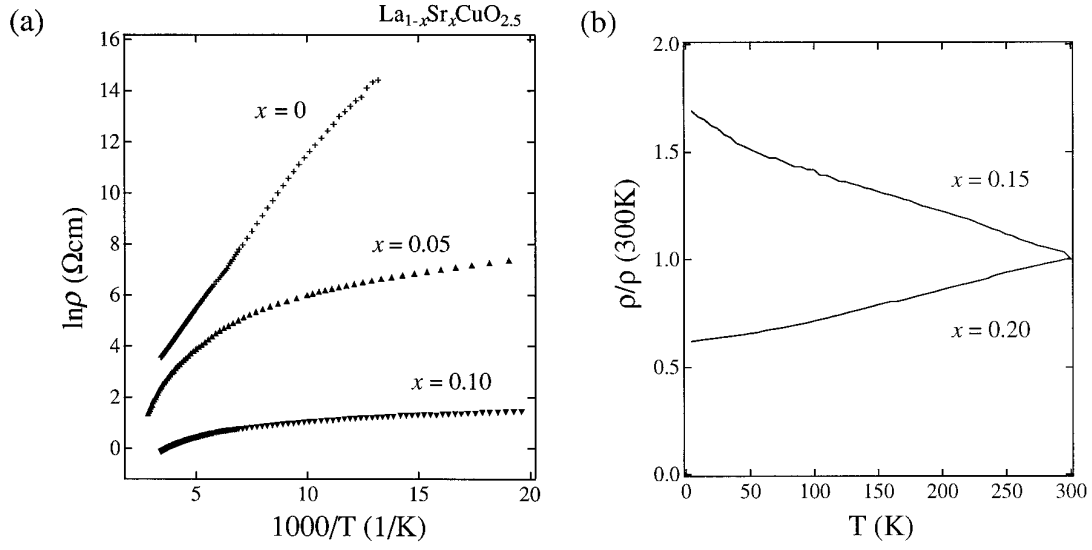

FIG. 15. Arrhenius plot, ln ρ vs $1/T$, for $x = 0.0$, 0.05, and 0.10 (a) and temperature dependence of resistivity normalized at 300 K for $x = 0.15$ and 0.20 (b).

which is drawn with exact atomic positions based on the Rietveld refinements (26). The most important factor to affect the electronic and magnetic properties of these materials must be arrangements of Cu d_{x2-y2}–O $2p_\sigma$ orbitals. For clarity only the Cu d_{x2-y2} orbitals are schematically shown in the figures. As described before, the HP compound is characterized as linear O–Cu–O–Cu–O bonds with their Cu d_{x2-y2} orbital planes perpendicular to the basal plane. In contrast, commonly observed in the $(La_{1-y}Sr_y)_8Cu_8O_{20}$ phase and also other perovskite-type phases in the (La, Sr)–Cu–O system is a mixture of two orientations of CuO_4 squares, perpendicular and parallel to the basal plane. One would expect from such an arrangement that metallic conduction can easily occur within the basal plane (and so three-dimensionally), because the in-plane Cu d_{x2-y2} orbitals would work as a terminal for electron transfer. This is apparently not the case for $La_{1-x}Sr_x$ $CuO_{2.5}$. The above consideration gives a reasonable explanation for the experimental facts that the $(La_{1-y}Sr_y)_8$ Cu_8O_{20} phase is always a good (three-dimensional) metal independent of x, whereas the HP $La_{1-x}Sr_x$ $CuO_{2.5}$ phase is more semiconductor-like, suggesting a reduced dimensionality of the HP phase. The reason why $CaMnO_{2.5}$-type $La_{0.857}Sr_{0.143}CuO_{2.5}$ was reported to show metallic conductivity (28) may be attributed to imperfect order of oxygen atoms or excess oxygens locating within the basal plane, which would trigger 3D conduction just as in $(La_{1-y}Sr_y)_8Cu_8O_{20}$.

Description of the structure. The structural refinement using the Rietveld method has been carried out for $x = 0.20$. The atomic coordinates of the nondoped compound were used as a starting point. For the refinement of the La and Sr occupancies a constraint $g(\mathrm{La}) + g(\mathrm{Sr}) = 1$ was imposed, assuming a statistical distribution of La and Sr. The final results of the fitting are summarized in Table 2. The fitting was fairly good, giving low R factors; $R_{wp} = 3.9\%$, $R_R = 9.0\%$, $R_e = 3.5\%$, and $S = 1.10$. The refined occupancy for Sr was 0.184(7), which was close to the nominal composition. A considerable peak broadening due to strain effect was detected, which might be attributed to microscopic inhomogeneity in Sr concentration, inevitable for a solid–solution system.

The changes in some important atom distances and angles on doping are shown by comparing those for $x = 0$ and 0.20 in Table 3. The Cu–Cu distances in the ladder along the leg and rung become shorter on doping by 0.39 and 0.99%, respectively, while that between adjacent ladders decreases by 0.34%. The ladder plane is almost flat in each compound. What significantly happens on doping is the rotation of rigid ladders which causes the increase in the angle between adjacent ladder planes, the decrease in the Cu–O(apex) distance, and also the decrease in the lattice parameter b. These results indicate that the quasi-one-dimensional structure is kept for doping.

Low-temperature XRD measurements for $La_{0.8}Sr_{0.2}$ $CuO_{2.5}$ revealed that no structural transitions occurred down to 10 K same as in the nondoped compound. The change of the lattice parameters is plotted in Fig. 8. As a result of doping, the lattice becomes soft along the a and b axes, but hard along the c axis. Since c directly measures the Cu–Cu bond along the leg, this means a strong metallic bond is formed along the ladder on doping.

Physical properties: resistivity. A dramatic insulator-to-metal transition has been observed with doping in the

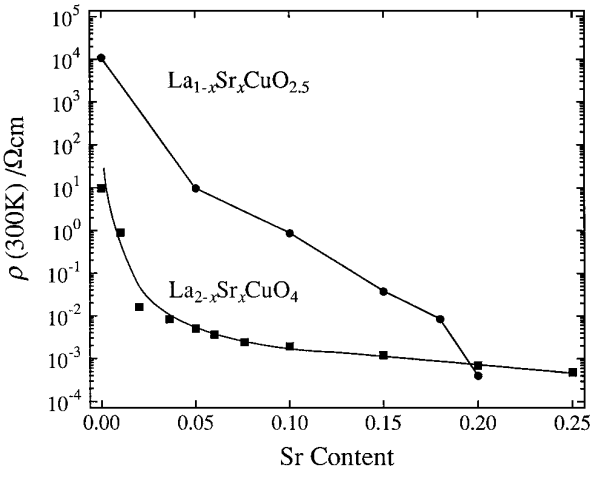

FIG. 16. Doping dependence of resistivity at 300 K for $La_{1-x}Sr_xCuO_{2.5}$ and $La_{2-x}Sr_xCuO_4$ (39, 42).

resistivity (ρ) measurements as shown in Fig. 14. Nondoped $LaCuO_{2.5}$ is almost insulative, while Sr doping systematically decreases the resistivity by more than seven orders of magnitude, and finally a metallic behavior down to 5 K is seen for $x = 0.20$. However, no indications of a superconducting transition have been seen for any doping level examined. The magnitude of resistivity for metallic $La_{0.8}Sr_{0.2}CuO_{2.5}$ is nearly the same as that of a superconductor $La_{1.8}Sr_{0.2}CuO_4$ in its normal state. The Arrhenius plot, ln ρ vs $1/T$, for $x = 0$ gave a straight line at high temperatures (Fig. 15a) from the gradient of which an activation energy of 1260 K (110 meV) was obtained. The temperature dependence for $0.05 \leq x \leq 0.15$ is rather weak: The resistivity gradually increases with decreasing temperature down to 5 K as typically shown for $x = 0.15$ in Fig. 15b. An insulator-to-metal transition occurs between $x = 0.15$ and 0.20. It is interesting to compare these results with the case of $La_{2-x}Sr_xCuO_4$ where metallic behavior appears for a much smaller hole concentration of $x \sim 0.01$ and superconductivity is observed for $x \geq 0.06$ (38, 39). Figure 16 compares the composition dependence of resistivity at 300 K between the two compounds. The distinct difference may reflect the essential difference in dimensionality between the two cuprates.

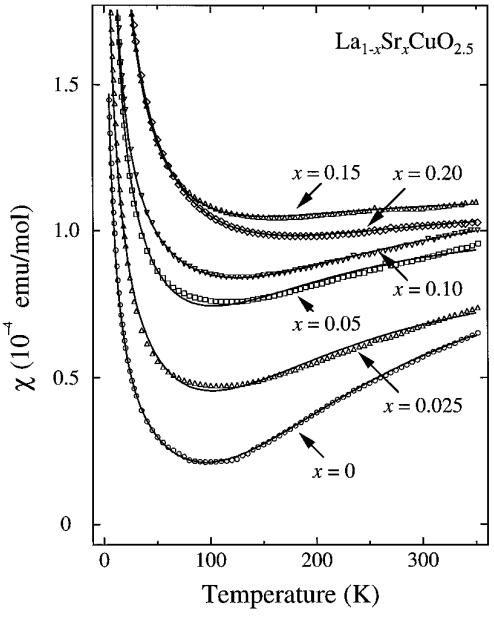

FIG. 17. Doping dependence of the magnetic susceptibility measured at an applied field of 1 T on heating after zero-field cooling. All the data sets are fitted to the equation in the text, the results of which are shown by the solid lines.

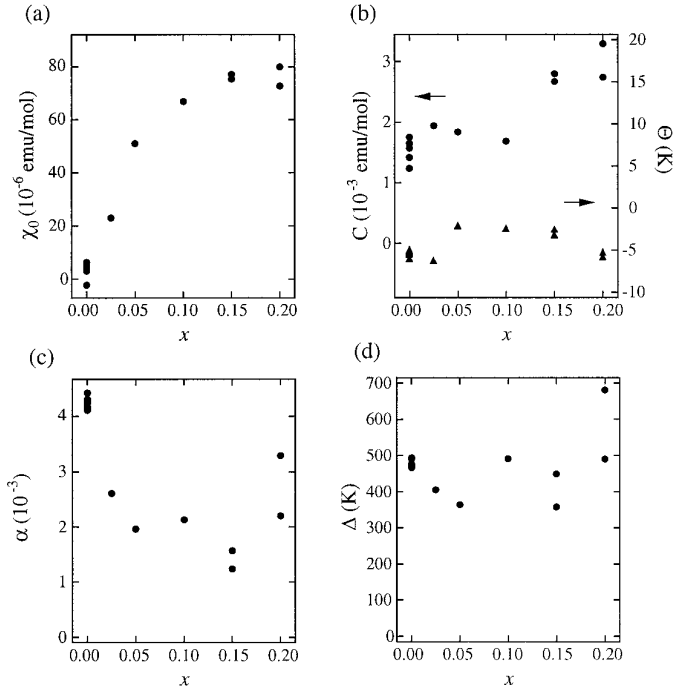

FIG. 18. Doping dependence of the parameters in the equation describing susceptibility for a spin-ladder system.

Magnetic susceptibility. The doping dependence of magnetic susceptibility is shown in Fig. 17. The magnitude increases with doping, and, at the same time, the characteristic decrease observed for $x = 0$ due to the presence of pseudo-gap seems to fade away gradually. Assuming the identical temperature dependence for pure and doped samples and fitting the data to the above equation, the doping dependence of all the parameters are calculated as summarized in Fig. 18. Apparently, χ_0 increases rapidly with doping. This may correspond to the evolution of an in-gap state which is responsible for the increase in conductivity. The Curie constant or the amount of free Cu ions increases only slightly.

CONCLUDING REMARKS

A new hole-doped spin-ladder compound $La_{1-x}Sr_xCuO_{2.5}$ has been studied. Unfortunately, the theoretical prediction of superconductivity in lightly doped spin ladders has not been confirmed in the present material. The main reason is that it is not good enough to realize the ideal spin-ladder model in the following two senses: One is that rather strong inter-ladder coupling prevents the parent material from having a well-defined spin gap. It should be addressed by theory how the singlet ground state is modified with increasing inter-ladder coupling. The other is that doped hole carriers tend to be localized probably because of the randomness in potential arising from the statistical mixing of aliovalent Sr^{2+} and La^{3+}. This partly reflects general difficulty in obtaining a 1D metal in a real material. In order to avoid such a localization effect it would be necessary to dope ladders with holes through chemical modification at faraway sites in more complicated crystal structures. Further experimental efforts to search for a new hole-doped spin-ladder compound are in progress.

ACKNOWLEDGMENTS

The author thanks M. Takano, H. Takagi, Y. Kitaoka, and T. M. Rice for helpful discussions. This study was supported by a Grant-in-Aid for Scientific Research on Priority Areas given by the Ministry of Education, Science, and Culture, Japan.

REFERENCES

1. E. Dagotto and T. M. Rice, *Science* **271,** 618 (1996).
2. D. J. Scalapino, *Nature* **377,** 12 (1995).
3. T. M. Rice, S. Gopalan, and M. Sigrist, *Europhys. Lett.* **23,** 445 (1993).
4. S. Gopalan, T. M. Rice, and M. Sigrist, *Phys. Rev. B* **49,** 8901 (1994).
5. S. R. White, R. M. Noack, and D. J. Scalapino, *Phys. Rev. Lett.* **73,** 886 (1994).
6. M. Azuma, Z. Hiroi, M. Takano, K. Ishida, and Y. Kitaoka, *Phys. Rev. Lett.* **73,** 3463 (1994).
7. K. Ishida, Y. Kitaoka, K. Asayama, M. Azuma, Z. Hiroi, and M. Takano, *J. Phys. Soc. Jpn.* **63,** 3222 (1995).
8. Z. Hiroi, M. Azuma, M. Takano, and Y. Bando, *J. Solid State Chem.* **95,** 230 (1991).
9. N. Kobayashi, Z. Hiroi, and M. Takano, submitted for publication.
10. K. Kojima, A. Keren, G. M. Luke, B. Nachumi, W. D. Wu, X. J. Uemura, M. Azuma, and M. Takano, *Phys. Rev. Lett.* **74,** 2812 (1995).
11. E. Dagotto, J. Riera, and D. Scalapino, *Phys. Rev. B* **45,** 5744 (1992).
12. T. Barnes, E. Dagotto, J. Riera, and E. S. Swanson, *Phys. Rev. B* **47,** 3196 (1993).
13. R. M. Noack, S. R. White, and D. L. Scalapino, *Phys. Rev. Lett.* **73,** 882 (1994).
14. C. A. Hayward, D. Poilblanc, R. M. Noack, D. L. Scalapino, and W. Hanke, *Phys. Rev. Lett.* **75,** 926 (1995).
15. F. C. Zhang and T. M. Rice, *Phys. Rev. B* **37,** 3759 (1988).
16. D. C. Johnston, J. W. Johnson, D. P. Goshorn, and A. J. Jacobson, *Phys. Rev. B* **35,** 219 (1987).
17. R. S. Eccleston, T. Barnes, J. Brody, and J. W. Johnson, *Phys. Rev. Lett.* **73,** 2626 (1994).
18. Z. Hiroi and M. Takano, *Nature* **377,** 41 (1995).
19. J. G. Bednorz and K. A. Müller, *Z. Phys. B* **64,** 189 (1986).
20. R. J. Cava, T. Siegrist, B. Hessen, J. J. Krajewski, W. F. P. Jr., B. Batlogg, H. Takagi, J. V. Waszczak, L. F. Schneemeyer, and H. W. Zandbergen, *Physica C* **177,** 115 (1991).
21. G. Demazeau, C. Parent, M. Pouchard, and P. Hagenmuller, *Mater. Res. Bull.* **7,** 913 (1972).
22. J. F. Bringley, B. A. Scott, S. J. LaPlaca, T. R. McGuire, F. Mehran, M. W. McElfresh, and D. E. Cox, *Phys. Rev. B* **47,** 15269 (1993).
23. H. Haas and E. Kordes, *Z. Kristallogr.* **129,** 259 (1969).
24. S. J. LaPlaca, J. F. Bringley, B. A. Scott, and D. E. Cox, *Acta Crystallogr. Sect. C* **49,** 1415 (1993).
25. D. M. DeLeeuw, C. A. H. A. Mutsaers, G. P. J. Geelen, and C. Langereis, *J. Solid State Chem.* **80,** 276 (1989).
26. L. Er-Rakho, C. Michel, and B. Raveau, *J. Solid State Chem.* **73,** 514 (1988).
27. K. Otzschi, K. Koga, and Y. Ueda, *J. Solid State Chem.* **115,** 490 (1995).
28. K. Otzschi and Y. Ueda, *J. Solid State Chem.* **107,** 149 (1993).
29. T. Siegrist, S. M. Zahurac, D. W. Murphy, and R. S. Roth, *Nature* **334,** 231 (1988).
30. M. Takano, Y. Takeda, H. Okada, M. Miyamoto, and K. Kusaka, *Physica C* **159,** 375 (1989).
31. Z. Hiroi, M. Azuma, M. Takano, and Y. Bando, *Physica C* **208,** 286 (1993).
32. F. Izumi, *in* "The Rietveld Method" (R. A. Young, Ed.), p. 236. Oxford Univ. Press, Oxford, 1993.
33. K. R. Poeppelmeier, M. E. Leonowicz, J. C. Scanlon, and J. M. Longo, *J. Solid State Chem.* **45,** 71 (1982).
34. M. Troyer, H. Tsunetsugu, and D. Warts, *Phys. Rev. B* **50,** 13515 (1994).
35. M. Kondo and M. Kubo, *J. Phys. Chem.* **62,** 1558 (1958).
36. S. Matsumoto, Y. Kitaoka, K. Ishida, K. Asayama, Z. Hiroi, N. Kobayashi, and M. Takano, *Phys. Rev. B* (1996) in press.
37. R. Kadono, J. Akimitsu, H. Okajima, A. Yamashita, K. Ishii, T. Yokoo, N. Kobayashi, Z. Hiroi, M. Takano, and K. Nagamine, submitted for publication.
38. J. B. Torrance, Y. Tokura, A. I. Nazzal, A. Bezinge, T. C. Huang, and S. S. P. Parkin, *Phys. Rev. Lett.* **61,** 1127 (1988).
39. H. Takagi, T. Ido, S. Ishibashi, M. Uota, S. Uchida, and Y. Tokura, *Phys. Rev. B* **40,** 2254 (1989).
40. M. Ogata, private communication.
41. D. M. DeLeeuw, C. A. H. A. Mutsaers, C. Langereis, H. C. A. Smoorenburg, and P. J. Rommers, *Physica C* **152,** 39 (1988).
42. S.-W. Cheong, J. D. Thompson, and Z. Fisk, *Physica C* **158,** 109 (1989).